C. R. Mecanique 340 (2012) 261–274

Contents lists available at SciVerse ScienceDirect

Comptes Rendus Mecanique

www.sciencedirect.com

Recent Advances in Micromechanics of Materials

Generalised continuum modelling of grain size effects in polycrystals

Nicolas M. Cordero, Samuel Forest *, Esteban P. Busso

MINES ParisTech, centre des matériaux, CNRS UMR 7633, BP 87, 91003 Evry cedex, France

ARTICLE INFO

Article history:
Available online 30 March 2012

Keywords:
Crystal plasticity
Strain gradient plasticity
Micromorphic theory
Kinematic hardening
Dislocation density tensor
Grain boundary
Polycrystalline aggregate
Hall–Petch effect

ABSTRACT

The effect of the dislocation density tensor is introduced into the classical crystal plasticity framework by means of the micromorphic theory of single crystals. A computational homogenisation strategy is presented in order to describe the global and local responses of two-dimensional polycrystalline aggregates for grain sizes ranging from 1 to 200 microns. The model is shown to naturally predict a size-dependent kinematic hardening behaviour which is responsible for the observed strong size effects. The yield stress at a given averaged plastic strain is shown to follow a power law scaling relation for grain sizes larger than a critical one. The field of plastic deformation is also strongly affected by grain size, whereby micron-size grains lead to the formation of intense slip bands crossing several grains.

1. Introduction

A long-standing problem in the modelling of polycrystal behaviour based on the knowledge of the constitutive behaviour of single crystals is the incorporation of grain size effects. Standard homogenisation procedures have shown to be capable of efficiently taking into account the grain-to-grain interaction primarily induced by strain incompatibilities at grain boundaries and grain morphology effects [1,2]. Continuum crystal plasticity models are available that satisfactorily describe dislocation forest hardening associated with multiplication and dynamic recovery of dislocation populations [3]. One strong limitation of these techniques is that the local crystal plasticity constitutive parameters at the grain scale are assumed to be known a priori. Conversely, these material parameters can be identified from the macroscopic polycrystal response by an inverse approach involving the homogenisation model. However, the resulting crystal plasticity model will be valid only for the considered grain size and thus the model can hardly be used for prediction of polycrystal behaviour for a different microstructure state, with different grain size and even morphology if grains are elongated in one direction.

Full-field models of polycrystals based on large-scale simulations of polycrystalline aggregates suffer from the same limitations [4]. Even though the intragranular mechanical fields, e.g. the plastic strain field, fulfilling all compatibility and equilibrium requirements are accurately computed, the simulation results are fundamentally size-independent. This means that homothetic polycrystal volumes subjected to the same mean strain will deliver the same mean stress and local stress field, in contradiction to the basics of physical metallurgy. Consequently, standard mean or full-field analyses of polycrystals are unable to account for the intrinsic grain size effect exhibited by small grains in materials with a bimodal distribution of grains [5]. Only the relative size effect is captured by such approaches.

The first attempt to restore the size-dependent character of crystal plasticity constitutive equations in the mean field approach of polycrystal behaviour goes back to [6] where a Hall–Petch relationship was explicitly introduced in the initial critical resolved shear stress in each grain. The limitation of this heuristic approach is that the Hall–Petch relationship

* Corresponding author.
E-mail address: samuel.forest@mines-paristech.fr (S. Forest).

1631-0721/$ – see front matter
doi:10.1016/j.crme.2012.02.009

should be an outcome of the model, not an input. Furthermore, the Hall–Petch correlation is a macroscopic relation which has no real physical meaning when written at the scale of each individual grain.

This fact has been recognised in more recent mean field approaches that rather resort to the three-phase self-consistent models whereby an interphase layer is introduced that accounts for the material grain boundary affected zone [7,5]. If a fixed size is attributed to this layer, varying the grain size amounts to modifying the boundary phase volume fraction and leads to different material responses. This strategy has been applied recently to the mechanics of nanocrystalline materials [8]. The idea of such grain boundary layer comes from the formation of dislocation pile-ups at grain boundaries at the early stages of plasticity. The existence of such a grain boundary affected zone is however not obvious and its determination requires the consideration of size-dependent intragranular plastic strain fields that are not provided by either such mean field models or by standard size-independent large-scale finite element simulations. In this work it will be shown that drastically different intragranular fields in terms of strain heterogeneities may develop as grain sizes decrease. It is also worth noting that the kinematic nature of hardening induced by pile-up formations is not considered in the pattern-based homogenisation approach, see [9].

It has been suggested in [10] that the influence of absolute grain size on the development of intragranular mechanical fields of polycrystalline aggregates can be modelled by linking the dislocation mean free path to the distance of crystal points to the closest grain boundary. In this way, the kinematic character of the internal stresses induced by pile-ups can be explicitly incorporated. However, in addition to the inherent technical difficulties associated with the determination of a suitable distance close to triple points or to free surfaces, the main limitation of this approach lies in the fact that after some deformation significant lattice rotation gradients develop leading to the formation of subgrain boundaries that also contribute to the overall size effects.

A more systematic and "implicit" way of triggering size-dependent internal stresses consists in relating them to the development of plastic strain gradients. Ideal dislocation pile-ups can be described by means of the dislocation density tensor, and the corresponding extra-hardening can be derived accordingly [11,12]. This remark suggests that the dislocation density tensor, computed as the curl of the plastic strain, should be introduced as a new constitutive variable in addition to the usual crystal plasticity internal state variables such as scalar dislocation densities. It is a size-dependent variable since it has the physical dimension of a strain gradient. Finite element simulations of the size-dependent response of polycrystalline aggregates have been presented in [13,14] by introducing extra-hardening induced by the dislocation density tensor or, equivalently, by densities of the so-called geometrically necessary dislocations (GND). However, this approach must be complemented by the introduction of an averaging procedure for the evaluation of plastic strain gradients in order to avoid spurious mesh dependency inherent to such an approach [15]. This undesired effect is due to the fact that no energy penalty exists in the formulation to limit the growth of gradients when refining the mesh. This limitation can be addressed by the incorporation of higher order stresses corresponding to the additional energy contributions required to penalise gradient terms.

Generalised continuum approaches therefore arise as a suitable mechanical framework for formulating enhanced crystal plasticity models that include the dislocation density tensor as a constitutive variable. Strain gradient plasticity started with the pioneering contribution of Aifantis [16], who introduced the Laplacian of plastic slip into the hardening rule. A second gradient theory inspired from Mindlin [17] was then formulated by Fleck and Hutchinson [18]. The link between the dislocation density tensor and lattice curvature according to Nye's relations prompted several authors in [19–23] to propose a Cosserat elasto-viscoplastic theory of single crystals whereby the Cosserat directors coincide with lattice vectors as initially suggested by Mandel [24]. The strain gradient theory was further developed by Gurtin [25,26] and encompasses previous models. Recent developments have shown the limitations of existing strain gradient models in the case of a two-phase laminate microstructure under single or double slip [27]. They plead for an even more general theory than the Cosserat approach, namely the micromorphic model inspired from Eringen [28] and extended to elasto-viscoplasticity in [29]. Strain gradient plasticity models have been used to compute polycrystalline aggregates with a small number of grains in [30,31], but no scaling law which accounts for grain size effects was derived.

The first objective of the present article is to propose a generalised continuum crystal plasticity model in order to predict Hall–Petch-like effects by means of finite element simulations of polycrystalline aggregates. The second objective is to show how intragranular deformation modes are influenced by grain size. The advantage of the numerical approach used in this work is that grain size can be varied with fixed grain morphology and texture so that theoretical scaling laws can be derived while isolating grain size effects from those of other variables. The drawback is that the current higher order constitutive equations are so simple that quantitative comparison can hardly be made with experimental results at that stage.

The retained generalised continuum model is depicted in Section 2. The periodic homogenisation strategy is described in Section 3. In Section 4 scaling laws for the overall stress are then derived as a function of overall strain and grain size. Finally, Section 5 is devoted to the description of the plastic strain field inside the polycrystals in terms of their grain size. The contribution ends with a discussion of the pros and cons of the proposed approach.

2. The *microcurl* model

The proposed model, so-called *microcurl*, is based on a micromorphic approach that falls in the class of the generalised continuum theories presented in [29]. The theory is first described in terms of the balance and constitutive equations within

the context of small deformation. A finite deformation formulation of the theory is available in [32]. Gurtin's strain gradient plasticity model will finally be shown to arise as a limiting case of the *microcurl* model [25].

2.1. Balance equations

We introduce a plastic micro-deformation variable, $\underset{\sim}{\boldsymbol{\chi}}^p$, as a second-rank generally non-symmetric tensor. The set of degrees of freedom of the theory is:

$$DOF = \left\{\underline{\boldsymbol{u}}, \underset{\sim}{\boldsymbol{\chi}}^p\right\} \tag{1}$$

The components of $\underset{\sim}{\boldsymbol{\chi}}^p$ are introduced as independent degrees of freedom. In the three-dimensional case, there are nine such components and the micro-deformation field is generally incompatible. We assume that only the curl part of the gradient of plastic micro-deformation plays a role in the power of internal forces, for reasons that will become apparent in Section 2.3:

$$p^{(i)} = \underset{\sim}{\boldsymbol{\sigma}} : \dot{\underset{\sim}{\boldsymbol{H}}} + \underset{\sim}{\boldsymbol{s}} : \dot{\underset{\sim}{\boldsymbol{\chi}}}^p + \underset{\sim}{\boldsymbol{M}} : \operatorname{curl} \dot{\underset{\sim}{\boldsymbol{\chi}}}^p \tag{2}$$

where $\dot{\underset{\sim}{\boldsymbol{H}}}$ is the velocity gradient, $\underset{\sim}{\boldsymbol{\sigma}}$ is the simple stress tensor, the relative stress $\underset{\sim}{\boldsymbol{s}}$ and the double stress tensor $\underset{\sim}{\boldsymbol{M}}$ are the stress tensors conjugate to the plastic micro-deformation and its curl. The curl operator is defined in a Cartesian basis as:

$$\left(\operatorname{curl} \underset{\sim}{\boldsymbol{\chi}}^p\right)_{ij} = \epsilon_{jkl} \chi^p_{ik,l} \tag{3}$$

The total power of internal forces over the domain V is then given by

$$\begin{aligned}
\mathcal{P}^{(i)} &= \int_V p^{(i)} \,\mathrm{d}V = \int_V \left(\underset{\sim}{\boldsymbol{\sigma}} : \dot{\underset{\sim}{\boldsymbol{H}}} + \underset{\sim}{\boldsymbol{s}} : \dot{\underset{\sim}{\boldsymbol{\chi}}}^p + \underset{\sim}{\boldsymbol{M}} : \operatorname{curl} \dot{\underset{\sim}{\boldsymbol{\chi}}}^p\right) \mathrm{d}V \\
&= \int_V \left((\sigma_{ij}\dot{u}_i)_{,j} + \left(M_{ij}\epsilon_{jkl}\dot{\chi}^p_{ik}\right)_{,l}\right) \mathrm{d}V + \int_V \left(-\sigma_{ij,j}\dot{u}_i + s_{ij}\dot{\chi}^p_{ij} - \epsilon_{jkl}M_{ij,l}\dot{\chi}^p_{ik}\right) \mathrm{d}V \\
&= -\int_V \sigma_{ij,j}\dot{u}_i \,\mathrm{d}V - \int_V \left(\epsilon_{kjl}M_{ik,l} - s_{ij}\right)\dot{\chi}^p_{ij} \,\mathrm{d}V + \int_{\partial V} \sigma_{ij}n_j\dot{u}_i \,\mathrm{d}S + \int_{\partial V} \epsilon_{jkl}M_{ij}n_l\dot{\chi}^p_{ik} \,\mathrm{d}S
\end{aligned}$$

where ϵ_{ijk} is the third order permutation tensor. The method of virtual power is used to derive the generalised balance of momentum equations. Assuming no volume forces for simplicity, one finds

$$\operatorname{div} \underset{\sim}{\boldsymbol{\sigma}} = 0, \qquad \operatorname{curl} \underset{\sim}{\boldsymbol{M}} + \underset{\sim}{\boldsymbol{s}} = 0 \tag{4}$$

The corresponding boundary conditions are:

$$\underline{\boldsymbol{t}} = \underset{\sim}{\boldsymbol{\sigma}}.\underline{\boldsymbol{n}}, \qquad \underline{\boldsymbol{m}} = \underset{\sim}{\boldsymbol{M}}.\underset{\sim}{\boldsymbol{\epsilon}}.\underline{\boldsymbol{n}} \tag{5}$$

where $\underline{\boldsymbol{t}}$ and $\underline{\boldsymbol{m}}$ are the simple and double tractions at the boundary, respectively.

2.2. Constitutive equations

The gradient of the displacement field is decomposed into its elastic and plastic contributions

$$\underset{\sim}{\boldsymbol{H}} = \underline{\boldsymbol{u}} \otimes \nabla = \underset{\sim}{\boldsymbol{H}}^e + \underset{\sim}{\boldsymbol{H}}^p \tag{6}$$

The elastic and plastic strains are the symmetric parts of $\underset{\sim}{\boldsymbol{H}}^e$ and $\underset{\sim}{\boldsymbol{H}}^p$, respectively. The free energy function is assumed to have the following arguments:

$$\psi\left(\underset{\sim}{\boldsymbol{\varepsilon}}^e, \quad \underset{\sim}{\boldsymbol{e}}^p := \underset{\sim}{\boldsymbol{H}}^p - \underset{\sim}{\boldsymbol{\chi}}^p, \quad \underset{\sim}{\boldsymbol{\Gamma}} := \operatorname{curl} \underset{\sim}{\boldsymbol{\chi}}^p\right) \tag{7}$$

where $\underset{\sim}{\boldsymbol{\varepsilon}}^e$ is the elastic strain tensor, $\underset{\sim}{\boldsymbol{e}}^p$ is the relative plastic strain that measures the difference between plastic deformation and the plastic micro-variable.

The entropy inequality is written as:

$$p^{(i)} - \rho\dot{\psi} \geqslant 0 \tag{8}$$

$$\left(\underset{\sim}{\boldsymbol{\sigma}} - \rho\frac{\partial\psi}{\partial\underset{\sim}{\boldsymbol{\varepsilon}}^e}\right) : \dot{\underset{\sim}{\boldsymbol{\varepsilon}}}^e - \left(\underset{\sim}{\boldsymbol{s}} + \rho\frac{\partial\psi}{\partial\underset{\sim}{\boldsymbol{e}}^p}\right) : \dot{\underset{\sim}{\boldsymbol{e}}}^p + \left(\underset{\sim}{\boldsymbol{M}} - \rho\frac{\partial\psi}{\partial\underset{\sim}{\boldsymbol{\Gamma}}}\right) : \dot{\underset{\sim}{\boldsymbol{\Gamma}}} + (\underset{\sim}{\boldsymbol{\sigma}} + \underset{\sim}{\boldsymbol{s}}) : \dot{\underset{\sim}{\boldsymbol{H}}}^p \geqslant 0 \tag{9}$$

The following state laws are adopted:

$$\underset{\sim}{\boldsymbol{\sigma}} = \rho \frac{\partial \psi}{\partial \underset{\sim}{\boldsymbol{\varepsilon}}^e}, \qquad \underset{\sim}{\boldsymbol{s}} = -\rho \frac{\partial \psi}{\partial \underset{\sim}{\boldsymbol{e}}^p}, \qquad \underset{\sim}{\boldsymbol{M}} = \rho \frac{\partial \psi}{\partial \underset{\sim}{\boldsymbol{\Gamma}}} \tag{10}$$

so that the residual intrinsic dissipation rate takes the form:

$$D = (\underset{\sim}{\boldsymbol{\sigma}} + \underset{\sim}{\boldsymbol{s}}) : \dot{\underset{\sim}{\boldsymbol{H}}}^p \geqslant 0 \tag{11}$$

Assuming a quadratic potential in Eq. (10), the following linear relationships are obtained:

$$\underset{\sim}{\boldsymbol{\sigma}} = \underset{\approx}{\boldsymbol{\Lambda}} : \underset{\sim}{\boldsymbol{\varepsilon}}^e, \qquad \underset{\sim}{\boldsymbol{s}} = -H_\chi \underset{\sim}{\boldsymbol{e}}^p, \qquad \underset{\sim}{\boldsymbol{M}} = A \underset{\sim}{\boldsymbol{\Gamma}} \tag{12}$$

where H_χ and A are the generalised micromorphic moduli. Note that the size effects exhibited by the solutions of boundary value problems involving such a model are related to an intrinsic length scale, typically defined as

$$l_\omega = \sqrt{\frac{A}{H_\chi}} \tag{13}$$

The flow rule can be derived from a viscoplastic potential, $\Omega(\underset{\sim}{\boldsymbol{\sigma}} + \underset{\sim}{\boldsymbol{s}})$, expressed in terms of the effective stress, $(\underset{\sim}{\boldsymbol{\sigma}} + \underset{\sim}{\boldsymbol{s}})$, that intervenes in the dissipation rate:

$$\dot{\underset{\sim}{\boldsymbol{H}}}^p = \frac{\partial \Omega}{\partial (\underset{\sim}{\boldsymbol{\sigma}} + \underset{\sim}{\boldsymbol{s}})} \tag{14}$$

For a single crystal admitting N slip systems, the kinematics of plastic deformation is dictated by the slip directions $\underline{\boldsymbol{m}}$ and the normal to the slip plane of each slip system:

$$\dot{\underset{\sim}{\boldsymbol{H}}}^p = \sum_{k=1}^{N} \dot{\gamma}^k \underline{\boldsymbol{m}}^k \otimes \underline{\boldsymbol{n}}^k \tag{15}$$

where $\dot{\gamma}^k$ is the slip rate. The dissipation takes then the form:

$$D = \sum_{k=1}^{N} \left(\tau^k + \underset{\sim}{\boldsymbol{s}} : \left(\underline{\boldsymbol{m}}^k \otimes \underline{\boldsymbol{n}}^k\right)\right) \dot{\gamma}^k \geqslant 0 \tag{16}$$

τ^k being the resolved shear stress on slip system k. A generalised Schmid criterion is postulated in the form

$$f^k(\underset{\sim}{\boldsymbol{\sigma}}) = \left|\tau^k + \underset{\sim}{\boldsymbol{s}} : \left(\underline{\boldsymbol{m}}^k \otimes \underline{\boldsymbol{n}}^k\right)\right| - \tau_c^k \tag{17}$$

where τ_c is the critical resolved shear stress. Accordingly, a back-stress component naturally arises in the yield function:

$$x^k := -\underset{\sim}{\boldsymbol{s}} : \left(\underline{\boldsymbol{m}}^k \otimes \underline{\boldsymbol{n}}^k\right) = (\operatorname{curl} \underset{\sim}{\boldsymbol{M}}) : \left(\underline{\boldsymbol{m}}^k \otimes \underline{\boldsymbol{n}}^k\right) = A(\operatorname{curl}\operatorname{curl} \underset{\sim}{\boldsymbol{\Gamma}}) : \left(\underline{\boldsymbol{m}}^k \otimes \underline{\boldsymbol{n}}^k\right) \tag{18}$$

after taking the balance equation (4) and the linear constitutive equation (12) into account.

2.3. Internal constraint

The modulus H_χ in Eq. (12) introduces a coupling between the macro- and micro-variables. It can also be interpreted as a penalty factor that constrains the relative plastic deformation $\underset{\sim}{\boldsymbol{e}}^p$ to remain sufficiently small. Equivalently, a high value of the coupling modulus, H_χ, forces the plastic micro-deformation to be as close as possible to the macroscopic plastic deformation tensor, $\underset{\sim}{\boldsymbol{H}}^p$. In the limit, the use of a Lagrange multiplier instead of the penalty factor, H_χ, is necessary to enforce the internal constraint that

$$\underset{\sim}{\boldsymbol{\chi}}^p \equiv \underset{\sim}{\boldsymbol{H}}^p \tag{19}$$

In that case, the curl of the plastic micro-deformation coincides with the curl of plastic deformation:

$$\operatorname{curl} \underset{\sim}{\boldsymbol{\chi}}^p \equiv \operatorname{curl} \underset{\sim}{\boldsymbol{H}}^p =: \underset{\sim}{\boldsymbol{\Gamma}} \tag{20}$$

which is known as the dislocation density tensor [33]. Accordingly, the proposed *microcurl* theory aims at introducing the effect of the dislocation density tensor into a single crystal plasticity constitutive framework. Note that when the internal constraint (19) is enforced, the *microcurl* model reduces to Gurtin's strain gradient plasticity model [25]. This strain gradient plasticity model will henceforth be referred to as the "*curl* H^p" model. In Eringen's and Mindlin's micromorphic theory,

the micro-deformation can be constrained to be as close as possible to the macro-deformation, represented by the usual deformation gradient tensor. Thus, the micromorphic model reduces to Mindlin's second gradient theory. We adopt here a similar constraint such that the *microcurl* model degenerates into Gurtin's strain gradient plasticity model. The curl of micro-deformation, $\underset{\sim}{\boldsymbol{\Gamma}}$, coincides with the dislocation density tensor only when this constraint is enforced. This suggests that, in the general unconstrained case, the micro-deformation $\underset{\sim}{\boldsymbol{\chi}}^p$ should not depart too much from the plastic deformation so that the $\underset{\sim}{\boldsymbol{\Gamma}}$ measure can still have the physical meaning of a dislocation density tensor. The departure of the micro-deformation from the plastic deformation introduces a new constitutive ingredient in the model that remains however of purely phenomenological nature.

The *microcurl* model also displays computational advantages compared to strain gradient plasticity models. In the latter models, the field equations are valid only in the domains of the body that are plastically deforming. Hence, the additional boundary conditions necessary for such a higher order theory need to be applied at the frontier between the elastic and plastic domains. Different techniques have been designed to track such a moving boundary in a body but they are computationally very expensive, see e.g. [34]. In the micromorphic model, the plastic micro-deformation is active everywhere in the body and boundary conditions hold for the geometrical boundaries of the body.

Note finally that, in the limiting case, the back-stress (18) arises naturally in the theory and is proportional to the second spatial derivatives of the plastic strain. This order of derivation is in accordance with the first proposal by Aifantis who introduced the Laplacian of plastic strain or plastic slip. In contrast, constitutive models incorporating extra-hardening proportional to the densities of geometrically necessary dislocations, directly related to the dislocation density tensor, involve the first gradient of either plastic strain [35] or plastic slip rates [36].

3. Periodic homogenisation of *microcurl* polycrystals

The computation of polycrystalline aggregates based on standard crystal plasticity models generally follows the rule of classical homogenisation theory in the sense that a mean strain is prescribed to a volume element of polycrystalline materials using suitable boundary conditions such as strain-based, stress-based or periodic ones. The structure of the boundary value problem is modified if a generalised continuum approach is used inside the considered volume element. To address the computational homogenisation of a heterogeneous *microcurl* medium of interest in this work, suitable boundary conditions for displacement and plastic micro-deformation must be defined. In the case of linear material behaviour, the structure of the unit cell problem to be solved can be derived from multiscale asymptotic expansion analysis. The resulting boundary conditions are then assumed to hold also for nonlinear material responses. Extending the asymptotic analysis performed in [37] for heterogeneous Cosserat media, we look for the displacement field $\underline{\boldsymbol{u}}$ and the plastic micro-deformation field $\underset{\sim}{\boldsymbol{\chi}}^p$ in the polycrystal volume element such that

$$\underline{\boldsymbol{u}}(\underline{\boldsymbol{x}}) = \underset{\sim}{\boldsymbol{E}} \cdot \underline{\boldsymbol{x}} + \underline{\boldsymbol{v}}(\underline{\boldsymbol{x}}), \quad \forall \underline{\boldsymbol{x}} \in V \tag{21}$$

with the fluctuation $\underline{\boldsymbol{v}}$ being periodic at homologous points of the boundary ∂V. Under these conditions the prescribed average strain is the symmetric second order tensor $\underset{\sim}{\boldsymbol{E}}$. The plastic micro-deformation $\underset{\sim}{\boldsymbol{\chi}}^p$ is periodic at homologous points of ∂V. As a result, the mean value of the micro-deformation gradient $\underset{\sim}{\boldsymbol{\Gamma}}$ vanishes.

The grain boundary conditions will be discussed next. At any interface of a *microcurl* continuum, there may exist some jump conditions for the degrees of freedom of the theory and the associated reactions, namely the simple and double traction vectors of Eq. (5). We consider in this work that such jumps do not exist. Instead, the displacement vector and the plastic micro-deformation tensor are assumed to be continuous at grain boundaries. As a result, the simple and double tractions (5) also are continuous. The continuity of plastic micro-deformation is then a new grain boundary condition that does not exist in classical crystal plasticity. It will generate boundary layers at grain boundaries which are essential for the prediction of size effects [27]. Consider now a grain boundary between a plastically deforming grain and an elastic grain where plasticity is not triggered. The continuity condition of plastic micro-deformation implies that it should vanish at this grain boundary, thus leading to a decrease of plastic slip associated with pile-up formation close to the grain boundary. More generally continuity of plastic micro-deformation is enforced at grain boundaries. Also grain boundaries are assumed to transmit simple and double tractions. Note that jump conditions or more specific interface laws may well be more realistic or physically motivated but they would require additional considerable computational effort. We believe that continuity conditions carry the main physical ingredient required to capture the targeted size effects in plasticity.

The simulations are limited to two–dimensional crystals under plane strain conditions, and a mean shear strain E_{12} is prescribed to the volume elements. Three different volume elements are considered, made of 52, 47 and 55 grains, respectively, according to a 2D Voronoi tessellation with periodic geometry, as shown in Fig. 1. The three statistical realisations of the material's microstructure have different grain shapes and orientations chosen randomly. Homothetic volumes constructed from the three previous volume elements will be considered, thus having different mean grain sizes but the same grain morphology and crystallographic texture.

Only two planar slip systems are considered in most simulations of this work. The slip directions and normal to the slip planes are contained within the considered plane of simulation. They are separated by the angle 2ϕ with $\phi = 35.1^\circ$ following [38]. The more general case of FCC crystals with 12 slip systems is addressed in Section 6.

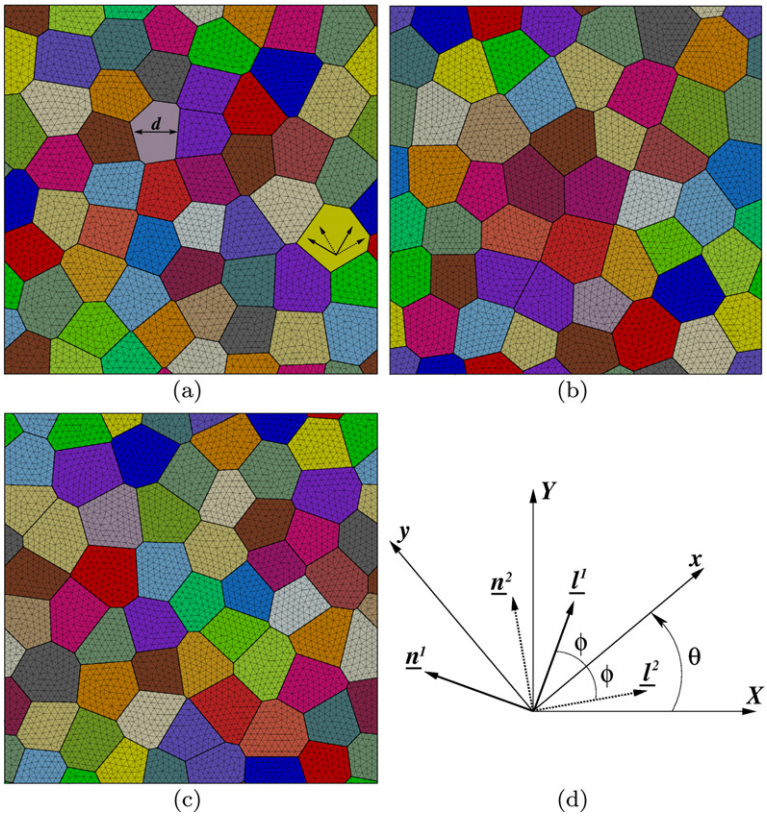

Fig. 1. Periodic meshes of the 2D periodic aggregates used in the finite element simulations: (a) 52 grains, (b) 47 grains and (c) 55 grains. Two slip systems are taken into account in each randomly oriented grain. Various mean grain sizes, d, ranging from tens of nanometres to hundreds of microns, are investigated. (d) Description of the two effective slip systems for 2D planar double slip.

Table 1
Set of material parameters used to retrieve the "*curl* H^p" model.

μ [MPa]	τ_c [MPa]	Q [MPa]	b	$h^{\alpha\alpha}$	$h^{\alpha\beta,\alpha\neq\beta}$	H_χ [MPa]	A [MPa mm^2]	l_ω [μm]
27 000	0.75	7.9	10.2	1	4.4	5.0×10^7	1.0×10^{-2}	1.5×10^{-2}

Table 2
Set of material parameters used in the finite element simulations corresponding to the *microcurl* model.

μ [MPa]	τ_c [MPa]	Q [MPa]	b	$h^{\alpha\alpha}$	$h^{\alpha\beta,\alpha\neq\beta}$	H_χ [MPa]	A [MPa mm^2]	l_ω [μm]
27 000	0.75	7.9	10.2	1	4.4	5.0×10^4	1.0×10^{-2}	4.5×10^{-1}

Two sets of material parameters are considered for the simulations, see Tables 1 and 2. The values are only loosely related to those typically encountered in FCC single crystals like aluminium and copper, with the following isotropic hardening rule:

$$\tau_c^r = \tau_c + Q \sum_{s=1}^{N} h^{rs}\left(1 - \exp\left(-b\gamma^s\right)\right) \tag{22}$$

where τ_c, Q, b and h^{rs} are material parameters. Isotropic elasticity is used for simplicity, the shear modulus being given in the tables and the Poisson ratio taken as $\nu = 0.3$.

The two sets of parameters considered here differ only by the choice of higher order moduli. A high value of the penalty parameter H_χ is taken in Table 1 so that the corresponding *microcurl* model almost coincides with the "*curl* H^p" model (see Section 2.3). The chosen parameter A is taken so that the constitutive length, l_ω, is equal to 15 nm. Note that this intrinsic length is defined from the ratio of two constitutive moduli for reasons of dimensionality. The resulting characteristic thickness of boundary layers affected by the strain gradient effects, especially close to grain boundary, will generally be proportional to l_ω with a factor depending on other constitutive parameters and on the type of boundary value problem. Such characteristic lengths have been derived from analytical solutions in some simple boundary value problems in [27]. For polycrystals, they will emerge from the computational analysis.

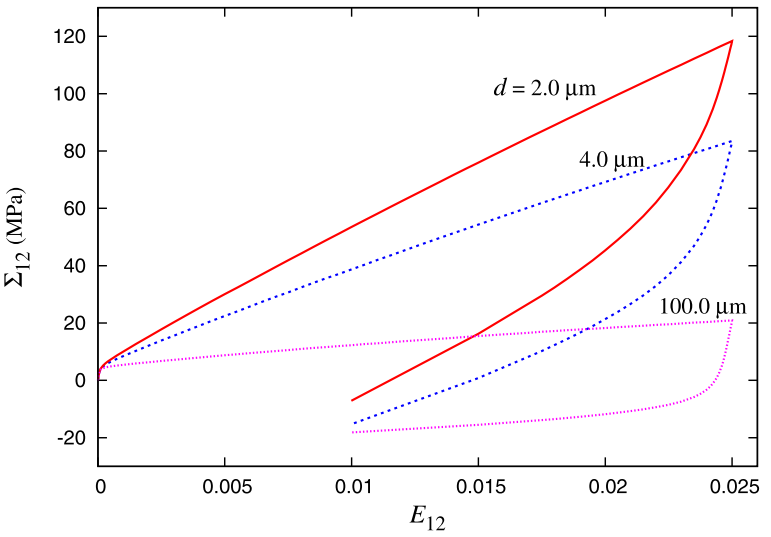

Fig. 2. Macroscopic stress–strain response of the 52-grain aggregate of Fig. 1(a) under simple shear loading–unloading conditions for three different grain sizes. The set of material parameters used are those given in Table 2.

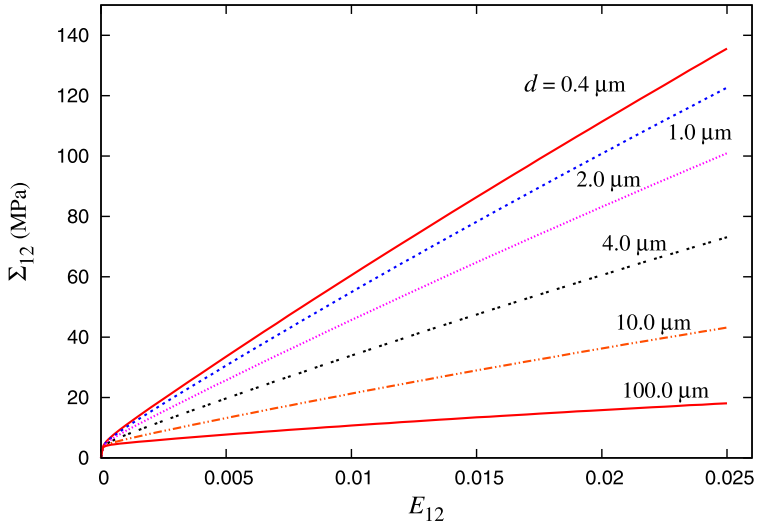

Fig. 3. Averaged macroscopic stress–strain response of the considered aggregates under simple shear for various mean grain sizes, d. The set of material parameters used are those given in Table 2.

As suggested in [27], the parameter H_χ can also be regarded as a constitutive parameter characterising specific properties of the materials. The way this parameter affects the prediction of grain size effects will be presented in the next section. A value $H_\chi = 50\,000$ MPa and a constitutive length $l_\omega = 450$ nm are considered in Table 2 after following an identification procedure explained in Section 4.

4. Scaling laws

4.1. Evidence of size-dependent kinematic hardening

Fig. 2 gives the mean shear stress as a function of mean shear strain for three different grain sizes, resulting from a finite element simulation of the 52-grain aggregate of Fig. 1(a) computed with the set of material parameters of Table 2. It shows the shear loading stage up to 0.025 mean shear strain followed by an unloading stage to 0.01. The stress–strain curves clearly exhibit an overall kinematic hardening effect induced by the local contributions of the back-stress, Eq. (18). The kinematic hardening vanishes for large grains and increases as the grain size decreases.

The effective quasi-linear hardening induced by strain gradient effects is also visible in Fig. 3 which shows monotonic shear loading curves for grain sizes ranging from 0.4 µm to 100 µm. For large grain sizes, almost flat curves are obtained,

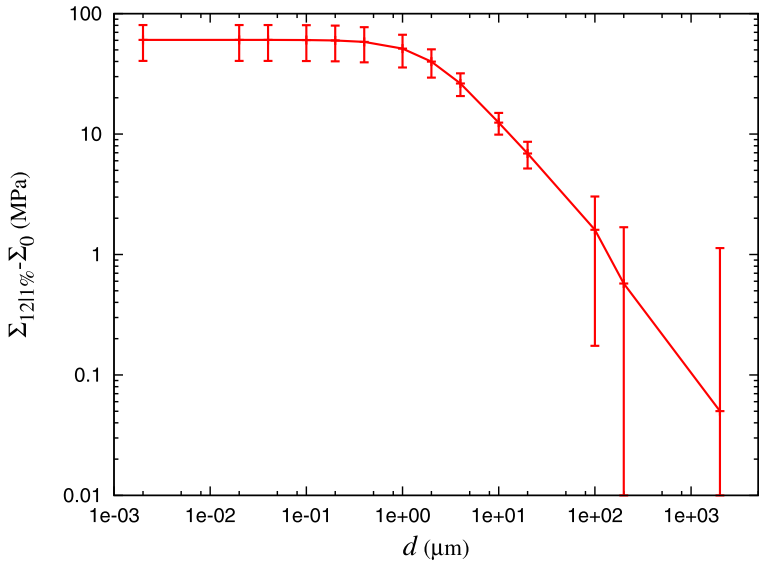

Fig. 4. Effect of the mean grain size, d, on the macroscopic flow stress $\Sigma_{12|1\%}$ at 1% mean plastic strain. The results are obtained with the three aggregates of Fig. 1 subjected to simple shear for the material parameters given in Table 2. The error bars give the results' standard deviation.

which corresponds to perfect plasticity since no classical hardening was introduced. It follows that the predicted strain hardening is of pure size-dependent nature. The effective linear kinematic hardening modulus is controlled by the higher order modulus A of the linear constitutive equation linking the gradient of the micro-deformation to the double stress tensor, see Eq. (12).

4.2. Size dependence of the overall shear stress at a given mean plastic strain

From the overall shear curves of Fig. 3, the shear stress value $\Sigma_{12|p_0}$ was recorded at a given level of mean plastic microstrain $\chi_{12}^{ps} = p_0$ where χ_{12}^{ps} is defined as:

$$\chi_{12}^{ps} = (\chi_{12}^{p} + \chi_{21}^{p})/2 \tag{23}$$

In Fig. 4, the mean shear stress $\Sigma_{12|p_0}$ is plotted as a function of grain size. It can be seen that the shear stresses converge toward a fixed value Σ_0 for large grain sizes. This limit depends only on the value of the critical resolved shear stress entering the Schmid law and on the specific geometry and orientations of the considered polycrystalline aggregates. It is therefore possible to draw a Hall–Petch diagram which is a log–log plot of $\Sigma_{12|p_0} - \Sigma_0$ vs. the grain size d. Such a plot is given in Fig. 4 for $p_0 = 0.01$. The continuous line gives the mean value of the shear stress level for the three cases of the microstructure considered in Fig. 1 and with the set of parameters of Table 2. Error bars are also provided showing the scatter of the results which is rather large due to the small number of grains in each microstructure and the small number of aggregates. The diagram of Fig. 4 clearly shows two regimes in the relation between stress level and grain size. For grain sizes smaller than 1 µm, no dependence of the overall stress on grain size is observed. However, for grain sizes larger than 1 µm, a power law relationship is found in the form

$$\Sigma_{12|p_0} - \Sigma_0 \propto d^m \tag{24}$$

with an exponent m of the order of -0.9 for the mean curve in Fig. 4. It can therefore be stated that the *microcurl* model is able to account for grain size effects with a saturation for very small grain sizes.

The Hall–Petch diagrams corresponding to both sets of parameters of Tables 1 and 2 are compared in Fig. 5 for the 52-grain aggregate case of Fig. 1(a). The high coupling modulus H_χ in Table 1 is such that the plastic micro-deformation locally does not depart from the plastic deformation $\underset{\sim}{\boldsymbol{H}}^p$ by more than 0.5%, which draws the model close to Gurtin's strain gradient plasticity model predictions. In contrast, differences of 3% can exist locally when a smaller value of H_χ is used, as in Table 2. As a result, Fig. 5's Hall–Petch predictions differ in the sense that the saturation level is higher for the strain gradient plasticity model, and that saturation starts at smaller grain sizes. The power law exponent m is slightly higher for the strain gradient plasticity model even though it is still of the order of $m = -1$, which should be compared to the value $m = -0.8$ for the response of the 52-grain aggregate using the material parameters of Table 2. Note that the parameter H_χ in Table 2 was chosen such that the saturation of the size effect occurs at approximately 1 µm.

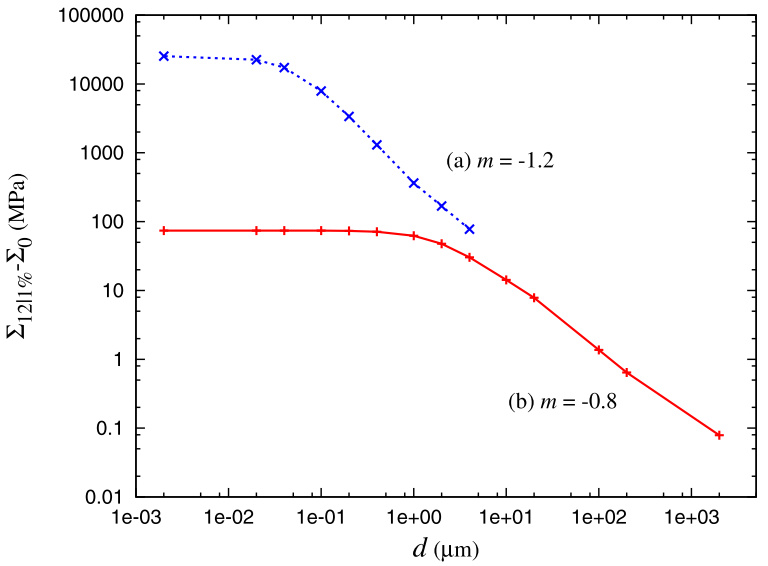

Fig. 5. Effect of the mean grain size, d, on the macroscopic flow stress $\Sigma_{12|1\%}$ at 1% mean plastic strain χ_{12}^{ps}. The results are obtained for the 52-grain aggregate of Fig. 1(a) under simple shear using the material parameters corresponding to (a) the "*curl* H^p" case given in Table 1, and (b) those given in Table 2.

5. Fields

The dislocation density tensor $\underset{\sim}{\boldsymbol{\Gamma}}$ does not only impact the overall polycrystal behaviour but also the way plastic deformation develops inside the grains. An example of the spreading of plastic deformation in a polycrystal depending on the grain sizes is shown in Fig. 6 for the 52-grain aggregate of Fig. 1(a). These contour plots show the field of equivalent plastic deformation p defined as

$$\dot{p} := \sqrt{\frac{2}{3}\underset{\sim}{\dot{\boldsymbol{H}}}^p : \underset{\sim}{\dot{\boldsymbol{H}}}^p} \tag{25}$$

At the onset of plastic deformation, plasticity starts in the same grains and at the same locations in 100-μm grains as in 1-μm grains, as shown in Fig. 6(a) and (b). This is due to the fact that the same critical resolved shear stress is adopted for both grain sizes, which corresponds to the same initial dislocation density. In contrast, at higher mean plastic strain levels, the strongly different values of the plastic micro-deformation gradients lead to significantly different plastic strain fields. Two main features are evidenced in Fig. 6(c) to (f). First, a tendency to strain localisation in bands is observed for small grain sizes. The plastic strain bands cross several grains whereas plastic strain is more diffuse at larger grain sizes, something which had already been seen in the simulations presented in [39,40]. Secondly, a consequence of this localisation is that some small grains are significantly less deformed than others, particularly the larger ones.

These features are also visible on the plastic deformation maps of Fig. 7 for the same aggregate but different grain sizes. This figure also shows the field of the norm of the dislocation density tensor:

$$\|\underset{\sim}{\boldsymbol{\Gamma}}\| := \sqrt{\underset{\sim}{\boldsymbol{\Gamma}} : \underset{\sim}{\boldsymbol{\Gamma}}} \tag{26}$$

This scalar quantity indicates the presence of GNDs and has the physical dimension of lattice curvature mm^{-1}. In large grains, GNDs are mainly located close to grain boundaries. At smaller grain sizes, the GND densities become significantly higher and spread over larger zones of the grains. Pile-up-like structures close to grain boundaries are clearly visible in the 10-μm grains.

The fact that strain gradient plasticity models may be prone to strain localisation when plasticity is confined in small regions was evidenced in [41] where intense slip bands were simulated in a perfectly plastic single crystal matrix around a hard particle. The matrix was modelled as a *microcurl* material. The reason for such a behaviour is that intense slip bands that exhibit a strong gradient of plastic slip perpendicular to the slip plane are not associated with GND formation. In contrast, regions of high lattice curvature or kink bands lead to an energy increase which is here quadratic with respect to $\underset{\sim}{\boldsymbol{\Gamma}}$ according to (12). This explains why, at a small scale, intense slip bands will be preferred to strongly curved regions and pile-ups. This is confirmed by the observation of the equivalent plastic deformation contour plots of Fig. 8 for the three aggregates considered in this work and for a grain size $d = 4$ μm. The orientation of the slip plane traces are indicated inside each grain. Here, the zones of intense plastic deformation are systematically found to be parallel to such slip plane traces, thus indicating the formation of slip bands during deformation.

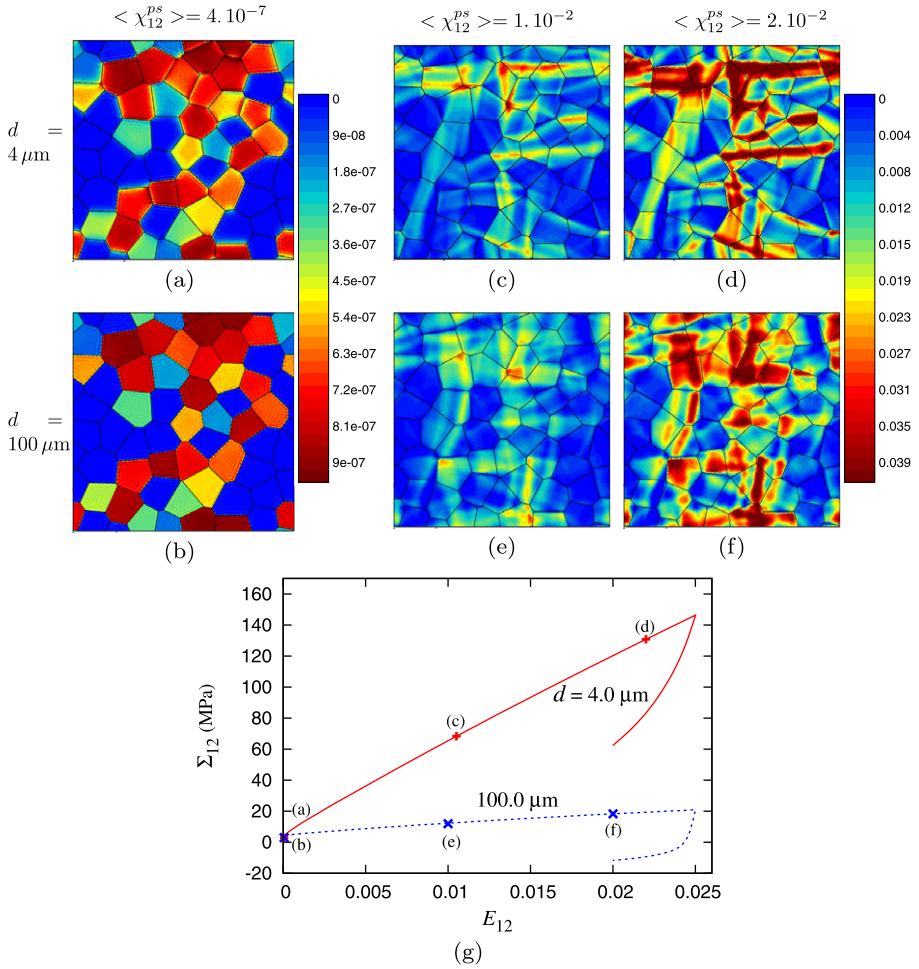

Fig. 6. (a)–(f) Contour plots of the accumulated plastic strain p for two grain sizes, $d = 100$ and 4 µm, and for three different mean values of the plastic strain: $\langle \chi_{12}^{ps} \rangle \approx 0$, $\langle \chi_{12}^{ps} \rangle = 0.01$ and $\langle \chi_{ps}^{12} \rangle = 0.02$, obtained with the 55-grain aggregate of Fig. 1(c) under simple shear and with the material parameters given in Table 2. (g) Macroscopic stress–strain response of the corresponding aggregate, with the letters indicating the different loading steps corresponding to the (a)–(f) contour plots.

6. Discussion

It is generally observed that strain gradient plasticity models provide a size-dependent hardening behaviour of polycrystals rather than a size-dependent initial yield stress [14,30]. Indeed in Fig. 3, the same initial yield stress can be read from the curves for all grain sizes whereas the hardening modulus is found to be strongly grain size-dependent. Since the overall shear curves result from the homogenisation of the polycrystalline unit cell of interest, we have defined a yield stress at 1% overall plastic strain which enabled us to plot Hall–Petch diagrams for the computed polycrystals. It should be emphasised that, even though the first plastic events start simultaneously for all homothetic polycrystals, the engineering yield stress at 0.2% will differ due to the fact that strain gradient effects strongly affect the microplasticity regime, as discussed in Section 5. Based on the proposed model, the microplasticity regime and the following hardening stage display the same size-dependent behaviour. This is due to the fact that a linear higher order constitutive equation has been chosen, see Eq. (12). A nonlinear constitutive law exhibiting saturation for higher values of the dislocation density tensors, would lead to a more pronounced size-dependent apparent initial yield stress followed by similar subsequent hardening behaviour. An analogous idea has been put forward in [42], whereby the effect of geometrically necessary dislocations may affect the local behaviour at the very beginning of microplasticity thus raising the yield strength. The authors in [42] propose a free energy function that depends on the norm of the dislocation density tensor leading to a singular derivative at zero initial density. This choice is different from the quadratic potential (12) retained in the present work. Future work must be dedicated to the development of more realistic higher order constitutive equations to better distinguish yield strength and hardening effects in strain gradient models.

In the present model, the dislocation density tensor is regarded as a state variable entering the free energy density function and does not directly contribute to the dissipation. More general nonlinear higher order constitutive equations

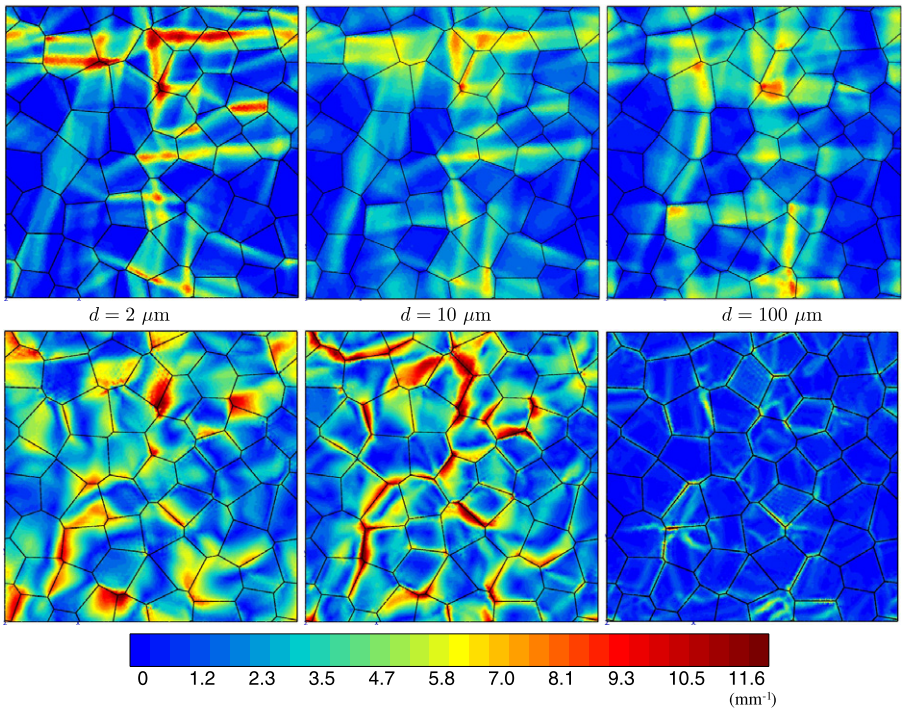

Fig. 7. Grain size effect on the accumulated plastic strain p (top figures) and on the norm of the dislocation density tensor $\|\underset{\sim}{\boldsymbol{\Gamma}}\|$ (bottom figures). These contour plots are obtained with the 55-grain aggregate for the same mean value of $\langle\chi_{12}^{ps}\rangle = 0.01$, and from the set of material parameters given in Table 2. The colour scale for the plastic strain field of the top figures is the same as that of Fig. 6 on the right. The colour scale at the bottom is that for the dislocation density tensor fields.

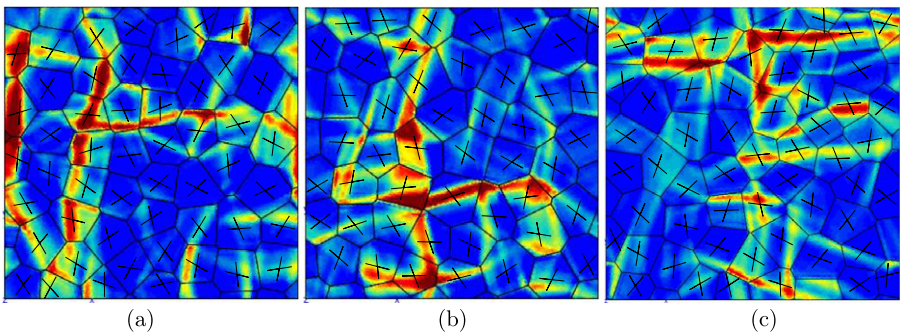

Fig. 8. Strain localisation patterns for a grain size $d = 4$ μm and for the three microstructures considered in Fig. 1. These contour plots are given for the same mean value of plastic strain $\langle\chi_{12}^{ps}\rangle = 0.01$, and for the set of material parameters given in Table 2. The pairs of slip plane traces are indicated inside each grain.

should incorporate a split of the strain gradient effect into separated energetic and dissipative contributions, as suggested in [29,26]. There are several ways of doing so: by splitting the stresses into its reversible and viscous parts as in [26], or by partitioning the strain measures as in [29]. However, additional parameters need to be introduced, which requires new identification strategies.

Single crystals with two slip systems are expected to be rather stiff compared to actual FCC crystals with twelve slip systems. To address the question as to the size effects persist when many slip systems are available to accommodate strain incompatibilities in the polycrystals, finite element simulations of plane strain shear loading on the same 2D microstructures have been performed, considering twelve slip systems at each material point, and a random orientation in each grain. The same material parameters were used as in Table 2, assuming an isotropic interaction matrix. The results are shown in Fig. 9, in terms of the overall shear at 1% overall plastic strain for different grain sizes. It can be seen that a size effect is still predicted. However the extra-stress at smaller grain sizes is significantly smaller than seen in Fig. 3. Also the unloading stage is purely elastic in contrast to Fig. 4. The kinematic hardening effect is weakened by an increasing number of potentially active slip systems. It seems that the high number of slip systems provides ways of avoiding high back-stress components. Thus, this framework is well-suited to materials with limited activated slip systems or in cases where the plastic deformation

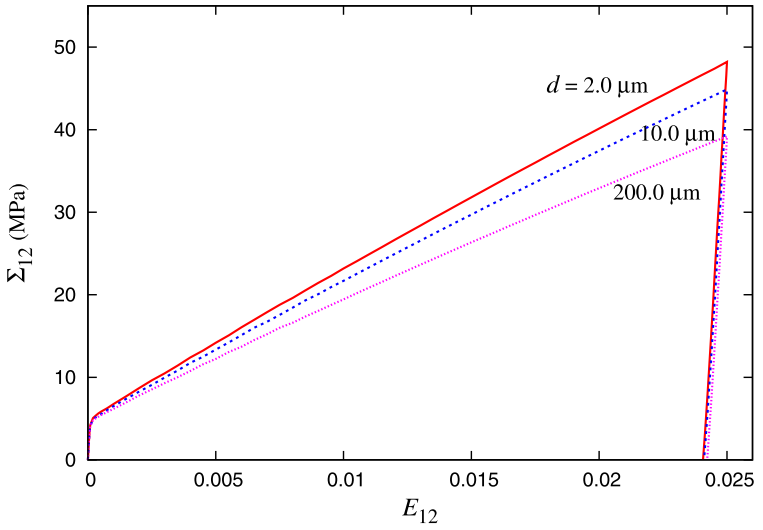

Fig. 9. Macroscopic stress–strain response of a 52-grain FCC crystal aggregate of Fig. 1(a) under simple shear and for FCC 12 slip systems potentially active.

is highly constrained. The question arises of the coupling between the different slip systems with respect to the computation of back-stresses. In the presence of multiple slip, the formula (18) has been kept which provides only an indirect coupling via the double stress tensor, the curl of which being projected on each slip system. It may well be necessary to consider the presence of an interaction matrix linking the various kinematic hardening components.

One essential feature of the presented *microcurl* model is the existence of a size-dependent kinematic hardening arising at each material point of the grains and leading to the observed overall kinematic hardening. This size-dependent hardening contribution comes in addition to more standard isotropic and kinematic hardening components contained in usual dislocation density-based crystal plasticity models. Explicit expressions of such back-stress components induced by dislocation pile-ups can be derived from dislocation theory and inserted into the constitutive model, as proposed in [43–45]. However they are limited to single slip situations in the absence of interaction with other dislocation populations. Such limitations motivate the need for the use of higher order constitutive formulations, such as that represented by Eq. (12). A linear relation like (12) is compatible with the dislocation model of single slip non-interacting pile-ups even though it is used here in the most general context.

7. Conclusions

The micromorphic crystal plasticity model proposed in this work represents an efficient compromise between sophisticated constitutive models incorporating the effect of so-called geometrically necessary dislocations, and phenomenological models allowing realistic finite element simulations of the mechanical behaviour of polycrystals. The curl of the micromorphic plastic deformation is used as a constitutive variable instead of the individual geometrically necessary dislocation densities. In that way, the same model can be used irrespective of the number of slip systems in the considered crystal structure. In contrast, models involving slips and/or individual dislocation densities for each slip system as new degrees of freedom will become computationally intractable in realistic situations. Furthermore, simple continuity rules for the microplastic deformation and tractions at grain boundaries were adopted. Such rules are independent again of the crystal structure and do not require complex additional interface conditions to be implemented. Even though they do not convey an exact physical description of dislocation processes at grain boundaries, it is our belief that they are more realistic than so-called micro-hard and micro-soft conditions directly applied at grain boundaries, see e.g. [31].

This work has shown that significant grain size effects can be observed in the simple shear response of 2D polycrystalline aggregates. They affect not only the overall hardening but also, in a non-trivial way, the plastic strain fields inside the grains. The two additional material parameters, A and H_χ, of the proposed *microcurl* model were shown to control the power of the scaling law and the grain size domain for which size effects occur. For ultra-fine grain sizes, plastic deformation was found to localise in intense slip bands that circumvent the formation of energetically expensive zones of high lattice curvature.

Future work is needed to more accurately estimate the scaling laws for the grain size dependency shown in this work. Currently, the power law exponents were found to be close to $m = -1$ from the 2D simulations with two slip systems. However, the high scatter in the responses due to the small number of grains in the simulations induces uncertainties in the evaluation of this exponent. More systematic and intensive computations are required. Future work will also be devoted to the development of more realistic nonlinear constitutive equations for the plastic micro-deformation gradient. Such laws could also be identified from the results of discrete dislocation dynamics simulations of various physical phenomena in two-phase materials and polycrystals [46,47,41] where strain gradients are significant.

Acknowledgements

This work is part of the NANOCRYSTAL project funded by the French National Research Council under contract ANR-07-BLAN-0186. Financial support of ANR is gratefully acknowledged. The second author wants to thank his former professor André Zaoui for helping him discover the world of research in the mechanics of materials.

References

[1] E. Sanchez-Palencia, A. Zaoui, Homogenization Techniques for Composite Media, Lecture Notes in Physics, vol. 272, Springer, Berlin, 1987.
[2] A. Zaoui, Continuum micromechanics: Survey, ASCE Journal of Engineering Mechanics 128 (2002) 808–816.
[3] B. Devincre, T. Hoc, L. Kubin, Dislocation mean free paths and strain hardening of crystals, Science 320 (2008) 1745–1748.
[4] G. Cailletaud, S. Forest, D. Jeulin, F. Feyel, I. Galliet, V. Mounoury, S. Quilici, Some elements of microstructural mechanics, Computational Materials Science 27 (2003) 351–374.
[5] J.M. Pipard, N. Nicaise, S. Berbenni, O. Bouaziz, M. Berveiller, A new mean field micromechanical approach to capture grain size effects, Computational Materials Science 45 (2009) 604–610.
[6] G.J. Weng, A micromechanical theory of grain-size dependence in metal plasticity, Journal of the Mechanics and Physics of Solids 31 (1983) 193–203.
[7] V. Marcadon, E. Hervé, A. Zaoui, Micromechanical modeling of packing and size effects in particulate composites, International Journal of Solids and Structures 44 (2007) 8213–8228.
[8] M. Cherkaoui, L. Capolungo, Atomistic and Continuum Modeling of Nanocrystalline Materials: Deformation Mechanisms and Scale Transition, Springer Verlag, 2009.
[9] R.J. Asaro, Elastic–plastic memory and kinematic hardening, Acta Metallurgica 23 (1975) 1255–1265.
[10] S. Lefebvre, Etude expérimentale et simulation numérique du comportement mécanique des structures sub-micrométriques de cuivre, PhD, Ecole Centrale Paris, 2006.
[11] S. Forest, R. Sedláček, Plastic slip distribution in two-phase laminate microstructures: Dislocation-based vs. generalized-continuum approaches, Philosophical Magazine A 83 (2003) 245–276.
[12] S. Forest, Some links between Cosserat, strain gradient crystal plasticity and the statistical theory of dislocations, Philosophical Magazine 88 (2008) 3549–3563.
[13] A. Acharya, A.J. Beaudoin, Grain size effects in viscoplastic polycrystals at moderate strains, Journal of the Mechanics and Physics of Solids 48 (2000) 2213–2230.
[14] K.S. Cheong, E.P. Busso, A. Arsenlis, A study of microstructural length scale effects on the behavior of FCC polycrystals using strain gradient concepts, International Journal of Plasticity 21 (2005) 1797–1814.
[15] C.F. Niordson, J.W. Hutchinson, On lower order strain gradient plasticity theories, European Journal of Mechanics A/Solids 22 (2003) 771–778.
[16] E.C. Aifantis, The physics of plastic deformation, International Journal of Plasticity 3 (1987) 211–248.
[17] R.D. Mindlin, N.N. Eshel, On first strain gradient theories in linear elasticity, International Journal of Solids and Structures 4 (1968) 109–124.
[18] N.A. Fleck, J.W. Hutchinson, Strain gradient plasticity, Advances in Applied Mechanics 33 (1997) 295–361.
[19] S. Forest, G. Cailletaud, R. Sievert, A Cosserat theory for elastoviscoplastic single crystals at finite deformation, Archives of Mechanics 49 (1997) 705–736.
[20] S. Forest, F. Barbe, G. Cailletaud, Cosserat modelling of size effects in the mechanical behaviour of polycrystals and multiphase materials, International Journal of Solids and Structures 37 (2000) 7105–7126.
[21] J.D. Clayton, D.J. Bamman, D.L. McDowell, A geometric framework for the kinematics of crystals with defects, Philosophical Magazine 85 (2005) 3983–4010.
[22] J.D. Clayton, D.L. McDowell, D.J. Bammann, Modeling dislocations and disclinations with finite micropolar elastoplasticity, International Journal of Plasticity 22 (2006) 210–256.
[23] J.R. Mayeur, D.L. McDowell, D.J. Bammann, Dislocation-based micropolar single crystal plasticity: Comparison of multi- and single criterion theories, Journal of the Mechanics and Physics of Solids 59 (2011) 398–422.
[24] J. Mandel, Equations constitutives et directeurs dans les milieux plastiques et viscoplastiques, International Journal of Solids and Structures 9 (1973) 725–740.
[25] M.E. Gurtin, A gradient theory of single-crystal viscoplasticity that accounts for geometrically necessary dislocations, Journal of the Mechanics and Physics of Solids 50 (2002) 5–32.
[26] M.E. Gurtin, L. Anand, Thermodynamics applied to gradient theories involving the accumulated plastic strain: The theories of Aifantis and Fleck & Hutchinson and their generalization, Journal of the Mechanics and Physics of Solids 57 (2009) 405–421.
[27] N.M. Cordero, A. Gaubert, S. Forest, E.P. Busso, F. Gallerneau, S. Kruch, Size effects in generalised continuum crystal plasticity for two-phase laminates, Journal of the Mechanics and Physics of Solids 58 (2010) 1963–1994.
[28] A.C. Eringen, Microcontinuum Field Theories, Springer, New York, 1999.
[29] S. Forest, The micromorphic approach for gradient elasticity, viscoplasticity and damage, ASCE Journal of Engineering Mechanics 135 (2009) 117–131.
[30] C.J. Bayley, W.A.M. Brekelmans, M.G.D. Geers, A three-dimensional dislocation field crystal plasticity approach applied to miniaturized structures, Philosophical Magazine 87 (2007) 1361–1378.
[31] S. Bargmann, M. Ekh, K. Runesson, B. Svendsen, Modeling of polycrystals with gradient crystal plasticity: A comparison of strategies, Philosophical Magazine 90 (2010) 1263–1288.
[32] O. Aslan, N.M. Cordero, A. Gaubert, S. Forest, Micromorphic approach to single crystal plasticity and damage, International Journal of Engineering Science 49 (2011) 1311–1325, http://dx.doi.org/10.1016/j.ijengsci.2011.03.008.
[33] B. Svendsen, Continuum thermodynamic models for crystal plasticity including the effects of geometrically-necessary dislocations, Journal of the Mechanics and Physics of Solids 50 (2002) 1297–1329.
[34] T. Liebe, A. Menzel, P. Steinmann, Theory and numerics of geometrically non-linear gradient plasticity, International Journal of Engineering Science 41 (2003) 1603–1629.
[35] H. Gao, Y. Huang, W.D. Nix, J.W. Hutchinson, Mechanism-based strain gradient plasticity – I. Theory, Journal of the Mechanics and Physics of Solids 47 (1999) 1239–1263.
[36] K.S. Cheong, E.P. Busso, Effects of lattice misorientations in FCC polycrystals, Journal of the Mechanics and Physics of Solids 54 (2006) 671–689.
[37] S. Forest, F. Pradel, K. Sab, Asymptotic analysis of heterogeneous Cosserat media, International Journal of Solids and Structures 38 (2001) 4585–4608.
[38] V.P. Bennett, D.L. McDowell, Crack tip displacements of microstructurally small surface cracks in single phase ductile polycrystals, Engineering Fracture Mechanics 70 (2003) 185–207.
[39] N.M. Cordero, S. Forest, E.P. Busso, S. Berbenni, M. Cherkaoui, Grain size effects on plastic strain and dislocation density tensor fields in metal polycrystals, Computational Materials Science 52 (2012) 7–13, http://dx.doi.org/10.1016/j.commatsci.2011.02.043.

[40] N.M. Cordero, S. Forest, E.P. Busso, S. Berbenni, M. Cherkaoui, Grain Size Effects in Generalised Continuum Crystal Plasticity, Wiley, 2011.
[41] H.J. Chang, A. Gaubert, M. Fivel, S. Berbenni, O. Bouaziz, S. Forest, Analysis of particle induced dislocation structures using three-dimensional dislocation dynamics and strain gradient plasticity, Computational Materials Science 52 (2012) 33–39, http://dx.doi.org/10.1016/j.commatsci.2011.02.014.
[42] N. Ohno, D. Okumura, Higher-order stress and grain size effects due to self-energy of geometrically necessary dislocations, Journal of the Mechanics and Physics of Solids 55 (2007) 1879–1898.
[43] C.J. Bayley, W.A.M. Brekelmans, M.G.D. Geers, A comparison of dislocation induced back stress formulations in strain gradient crystal plasticity, International Journal of Solids and Structures 43 (2006) 7268–7286.
[44] S. Berbenni, M. Berveiller, T. Richeton, Intra-granular plastic slip heterogeneities: Discrete vs. mean field approaches, International Journal of Solids and Structures 45 (2008) 4147–4172.
[45] C. Collard, V. Favier, S. Berbenni, M. Berveiller, Role of discrete intra-granular slip bands on the strain-hardening of polycrystals, International Journal of Plasticity 26 (2010) 310–328.
[46] S. Lefebvre, B. Devincre, T. Hoc, Yield stress strengthening in ultrafine-grained metals: A two-dimensional simulation of dislocation dynamics, Journal of the Mechanics and Physics of Solids 55 (2007) 788–802.
[47] F. Šiška, D. Weygand, S. Forest, P. Gumbsch, Comparison of mechanical behaviour of thin film simulated by discrete dislocation dynamics and continuum crystal plasticity, Computational Materials Science 45 (2009) 793–799.